RESEARCH PAPER

Electromagnetic Behavior of In-Situ Synthesized MXene-Based Ti_3C_2/TiO_2 Composites

Khshayar Zamani, Majid Tavoosi*, Ali Ghasemi

* *ma.tavoosi@gmail.com*

Department of Materials Engineering, Malek-Ashtar University of Technology (MUT), Iran

Received: May 2025 **Revised: July 2025** **Accepted: October 2025**
DOI: 10.22068/ijmse.4035

Abstract: *The present work was undertaken to study the effect of in-situ precipitation of TiO_2 from the $Ti_3C_2T_x$ MXene phase on the electromagnetic (EM) behaviour of Ti_3C_2/TiO_2 composites. In this regard, the $Ti_3C_2T_x$ MXene phase was synthesised using HF acidic etching of the Ti_3AlC_2 MAX phase, and the in-situ precipitation of the TiO_2 phase within the Ti_3C_2 sheets was followed by controlled annealing in a temperature range of 500-800°C for 2 h. The phase and structural characteristics of prepared composites were investigated using X-ray diffraction (XRD), scanning electron microscope (SEM) and differential thermal analysis. The electromagnetic behaviour of the samples was also analysed using a vector network analyser (VNA). The results showed that by performing the controlled annealing process of $Ti_3C_2T_x$ MXene phase, it is possible to in-situ formation of TiO_2 phase and create the Ti_3C_2/TiO_2 composites. The electromagnetic behaviour of Ti_3C_2/TiO_2 composites is in direct relation to the percentage of TiO_2 phase deposited within Ti_3C_2 sheets during the annealing process. The reflection loss (RL) changed from -7.98 to -21.28 dB (within frequency range of 1-18 GHz) with an increase in annealing temperature from 500 to 800°C, as well as an increase in the size and percentage of formed TiO_2 particles.*

Keywords: *MAX, MXene, In-situ, Composite, Electromagnetic.*

1. INTRODUCTION

High temperature electromagnetic wave absorbing materials, thanks to their wide applications, have attracted the attention of scientific research societies. These materials have secured their place in communication means/devices, as well as the aerospace industry and electronic equipment [1]. Besides exhibiting high performance in wave absorption, they should have very slight thickness, light weight and a wide frequency range [2]. Traditional wave-absorbing materials, including ferrites, metallic magnetic powders, conducting polymers, etc., faced limitations and did not meet these requirements. Hence, the development of new materials with unique properties, such as MAX and MXenes, was accelerated [3].

MXenes are known by the general formula of $M_{n+1}AX_n$ (n= 1, 2 or 3) generated by selective etching of MAX phase ceramics. In this formula, M is an intermediate metal, A is an element from group A (often an element from groups 3, 4 or 5 of the periodic table), X is nitrogen or carbon, and Tx represents superficial functional groups like -F, -OH, and -O [4, 5]. This group of materials, owing to their layered structure and a large number of native defects and chemically active surfaces, is the most apt candidate for EM interference shielding and absorption applications [6].

According to the literature, the shielding performance of MXenes can be enhanced by incorporating magnetic and dielectric reinforcing phases. However, dielectric reinforcement materials are more desirable for high temperature applications, as the magnetic properties of the material are lost at high temperatures [7-9]. In this regard, numerous research studies have been devoted to investigating MXene-based composites containing dielectric materials [10]. Among the dielectric absorbent materials, TiO_2 is a suitable candidate for high-temperature EM applications due to its stable dielectric properties and low density. Additionally, TiO_2 leads to an increase in $Ti_3C_2T_x$ MXene dielectric layers, thereby optimising impedance matching [11]. Moreover, TiO_2 can be deposited in situ inside the MXene layers during a controlled annealing [12-14].

In this regard, Fan et al. [15] reported that the precipitation of TiO_2 nanoparticles from $Ti_3C_2T_x$ during the annealing process has significant effects on EM absorption behaviours of prepared composites. In this research, the RL_{min} of the prepared $Ti_3C_2T_x/TiO_2$ composite was approximately 40.7 at a matching frequency of 19.2 GHz (thickness: 1.5 mm). In other work, Sun et al. [16] successfully grew TiO_2 particulates inside $Ti_3C_2T_x$ MXene layers using a hydrothermal

[DOI: 10.22068/ijmse.4035]

method and achieved a reflection loss of approximately 58.30 dB (1.75 mm thickness) in the optimised composite. Reports presented by Gao et al. [18] and Yan et al. [17] also show the positive effects of the presence of TiO_2 on EM behaviour of MXene-based composites within the band X boundary.

Despite the numerous studies about the preparation and different characteristics of MXene-based composites, no coherent report has yet been presented on the exact effect of TiO_2 on the EM behaviours of these composites. So, this research focused on the in-situ preparation of the TiO_2 phase within the Ti_3C_2 sheets during the controlled annealing process of the $Ti_3C_2T_x$ MXene phase. The most important goal of this work was to investigate the electromagnetic wave absorption behavior in the frequency range of L (1 to 2 GHz), S (2 to 4 GHz), C (4 to 8 GHz), X (8 to 12 GHz) and Ku (12 to 18 GHz) bands in the formed composites.

2. EXPERIMENTAL PROCEDURES

In this research, Ti_3AlC_2 MAX powder with a purity of above 99% and a mean particle size of less than 10 μm (REDOX Company) was used as raw material for the formation of MXene phase. The $Ti_3C_2T_x$ MXene phase was prepared using selective etching of Al from the Ti_3AlC_2 MAX powder in the Hydrofluoric acid (HF) (≥40 wt%, analysis) [11]. In a typical synthesis process, 2 g of the MAX powders were slowly added to 50 mL of HF solution. The etching process was continued for 24 hours [19], while stirring was facilitated with the aid of a magnetic bar. Afterwards, the mixture was washed several times with deionised water, whereupon centrifugation was performed at 3500 rpm for 5 min per cycle. After the last centrifuge, the pH of the supernatant was around 7.0. Subsequently, the product was washed with alcohol and dried in a vacuum oven at 60°C for 24 h [19]. The Ti_3C_2/TiO_2 composites were prepared during a controlled annealing process of the prepared $Ti_3C_2T_x$ MXene phase at a temperature range of 500-800°C for 2 h (under argon protective atmosphere).

Phase examinations of the obtained samples were conducted via X-ray diffraction (XRD) analysis using an XRD device (PW3710, Phillips Co.) at a voltage of 40 kV and a current of 0.05 amperes. Morphological characteristics of the powder samples were inspected through scanning electron microscopy (SEM) (VEGA-TESCAN-XMU, Czech Republic). The differential scanning calorimetry (DSC) analysis of the samples was also conducted using a STA 409 PC/PG device (NETZSCH Co.), under argon gas protection with the heating rate of 20°C/min. A PNA-5222A vector network analyzer (VNA) system was utilized for analyzing the electromagnetic waves absorption of the studied samples.

3. RESULTS AND DISCUSSION

The X-ray diffraction patterns of Ti_3AlC_2 MAX phase before and after etching process at HF solution for 24 h are shown in Fig. 1. A glance at the peaks formed in Fig. 1(a) at angles of 34.1, 36.8, 38.9, 41.9, and 74.2° based on the reference code (JCPDS:52-0875) indicates the formation of a high-purity Ti_3AlC_2 MAX phase and there is no evidence of impurities in this sample. Fig. 1(b) shows the XRD pattern of Ti_3AlC_2 MAX phase after selective etching of Al in HF solution for 24 h.

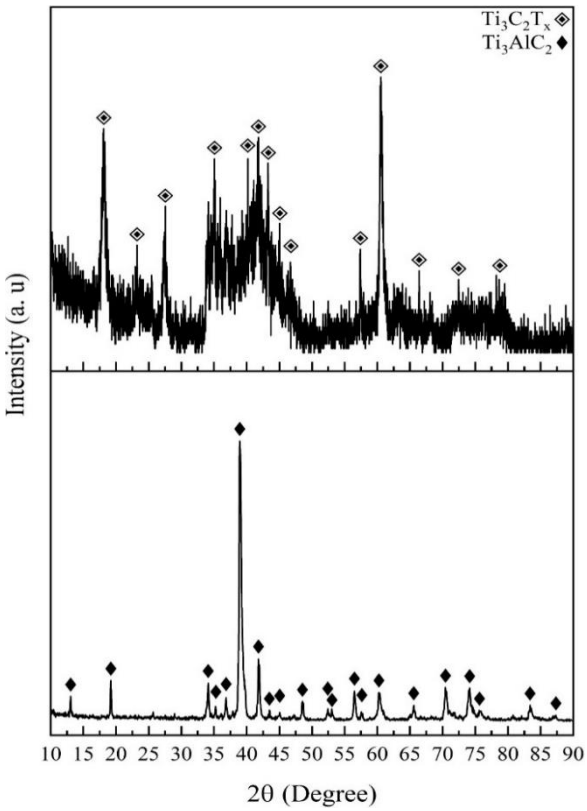

Fig. 1. X-ray diffraction patterns of Ti_3AlC_2 MAX phase a) before and b) after etching process in HF solution for 24 h

[DOI: 10.22068/ijmse.4035]

As can be clearly seen, the diffraction peaks corresponding to the Ti_3AlC_2 phase disappear entirely, and the XRD pattern is formed at angles of 18.5°, 35.9°, 41.7°, and 60.7°, corresponding to the characteristic peaks of the $Ti_3C_2T_x$ MXene phase [11, 20]. The latter result is confirmed by the SEM micrographs illustrated in Fig. 2, where the accordion-like multi-layered nano-flake $Ti_3C_2T_x$ MXene is clearly visible. The result obtained from the SEM image is consistent with those presented by Tong et al. [21].

To study the thermal behaviour of the prepared $Ti_3C_2T_x$ MXene phase, the sample was examined using the DSC technique under continuous heating. The DSC heating trace of this sample, in Fig. 3, reveals only one wide endothermic peak in the temperature range of 500-800°C. To analyse the phase transformation responsible for the endothermic peak, the $Ti_3C_2T_x$ MXene phase was annealed within 500, 600, 700 and 800°C for 2 h, and the samples were examined using the XRD technique. The XRD patterns of annealed samples are presented in Fig. 4. As seen, during annealing process, the diffraction peaks intensity corresponding to MXene phase gradually decrease and several new peaks related to TiO_2 phase with anatase at 25.1, 37.5, 48.12, 54.7, and 69.56° angles (JCPDS:21-1272) and TiO_2 phase with rutile at 27.4, 36.06, 41.22, 54.32, and 56.7° angles (JCPDS:21-1276) structures appear in XRD patterns. This finding is in agreement with those reported by Lei et al. [22]. Therefore, the endothermic peak in Fig. 3 should be attributed to the precipitation of TiO_2 from the $Ti_3C_2T_x$ MXene phase. In fact, the presence of -OH and -O groups on the surface of $Ti_3C_2T_x$ causes thermodynamic instability of MXene and leads to the in-situ formation of TiO_2 deposits during the annealing process [23, 24]. The following equations (1-5) can be proposed to explain the formation mechanism of Ti_3C_2/TiO_2 composite:

$TiO_2\ (e^- + h^+) + Ti_3C_2 \rightarrow TiO_2\ (h^+) + Ti_3C_2\ (e^-)$ (1)

$Ti3C2\ (h^+) + OH^- \rightarrow \bullet OH + TiO_2$ (2)

$Ti_3C_2\ (e^-) + O_2 \rightarrow \bullet O_2^- + TiO_2\ H_2O\bullet OH + Ti_3C_2$ (3)

$TiO_2\ (h^+) + OH^- \rightarrow \bullet OH + TiO_2$ (4)

$TiO_2\ (e^-) + O_2 \rightarrow \bullet O_2^- + TiO_2\ H_2O\bullet OH + TiO_2$ (5)

As mentioned, the diffraction patterns presented in Fig. 4 well confirm the in-situ formation of Ti_3C_2/TiO_2 composites. This result is in agreement with the presented SEM micrographs of annealed samples at 500, 600, 700 and 800°C in Fig. 5. Based on this figure, the nano-sized TiO_2 particles with unique distribution are formed on initial layers of MXene sheets. The morphology of the formed TiO_2 nanoparticles is close to spherical, and their size increases to approximately 180 nm with increasing annealing temperature.

The real parts of electrical permittivity (ε') and magnetic permeability (μ') indicate the potential for electrical and magnetic energy storage.

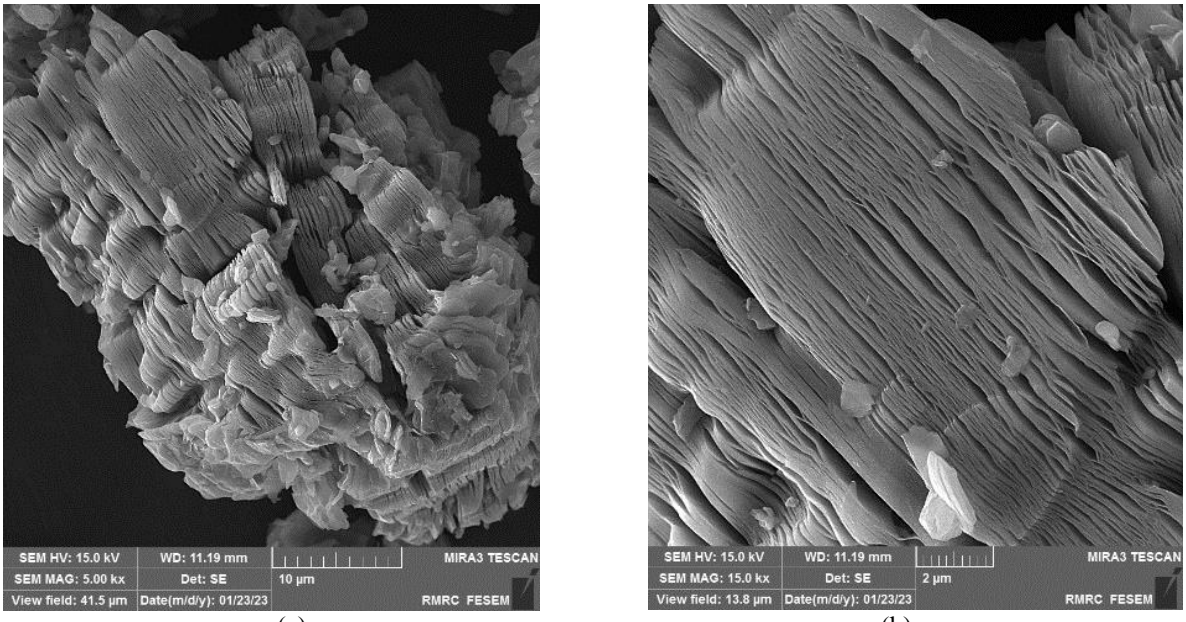

(a) (b)

Fig. 2. The SEM micrographs of Ti_3AlC_2 MAX phase after etching process in HF solution for 24 h (at two different magnifications)

[DOI: 10.22068/ijmse.4035]

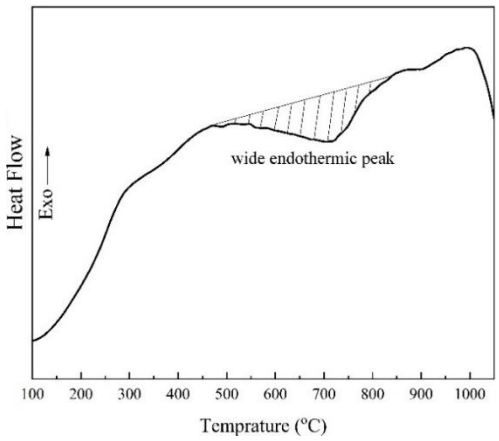

Fig. 3. The DSC heating trace of $Ti_3C_2T_x$ MXene phase

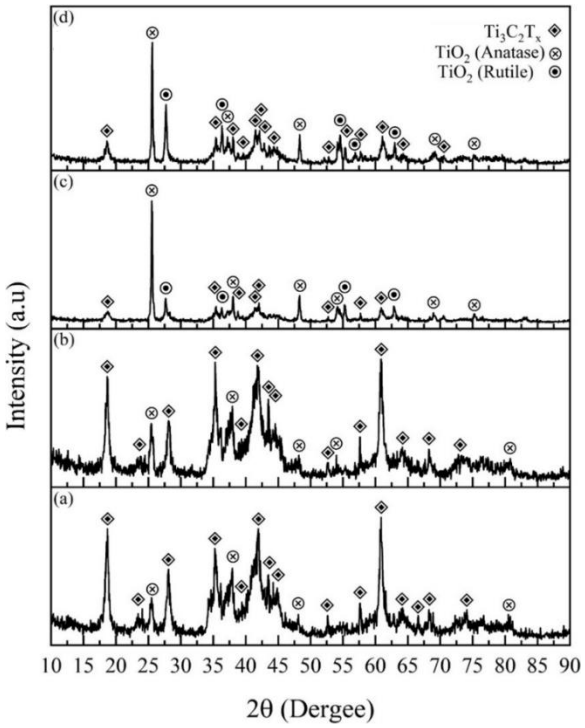

Fig. 4. X-ray diffraction patterns of $Ti_3C_2T_x$ MXene phase after annealing process at, a) 500, b) 600, c) 700 and d) 800°C for 2 h

Whereas imaginary parts show rate of electrical and magnetic energy loss [25]. The real (μ') and imaginary parts (μ″) of permittivity in prepared composites in this study are evaluated as approximately 1 and 0, respectively, as a result of the absence of magnetic components in the composition. But, the changes in imaginary and real parts of electrical permittivity in relation to frequency (within 1-18 GHz) for prepared composites at different annealing temperatures are illustrated in Fig. 6. Based on this figure, several points can be concluded as:

- The pure Ti_3C_2 MXene shows the highest values of real (ε') and imaginary part (ε") of electrical permittivity.
- By increasing the annealing temperature to 700°C, the real and imaginary parts of electrical permittivity decrease progressively. This point can be related to the change in MXene structure and precipitation of TiO_2 phase within the Ti_3C_2 layers during the annealing process.
- The changes in the imaginary and real parts of the electrical permittivity curves of the annealed samples at 700 and 800°C are the same. This means that increasing the temperature further than 700°C does not have a significant effect on the electrical permittivity of the resulting composites.
- The real and imaginary part of the electrical permittivity of the prepared composites follows a downward trend as the frequency increases from 1 to 18 GHz. This is related to reductions in eddy currents losses [9].

The attenuation coefficient (α) and skin depth (δ) are important parameters for evaluating the dissipating capacity and the microwave absorption capability of an electromagnetic wave absorber, respectively. The higher the attenuation coefficient of an absorber, the more electromagnetic wave energy can be converted into heat. The skin depth values also affect the ability to absorb EM waves. The thickness of the absorbing material must be greater than the skin depth in order to positively affect the absorption performance of EM waves. The changes in attenuation coefficient and skin depth versus the frequency for prepared composites are shown in Fig. 7. The presented results in Fig. 7 are calculated using the following equations [9, 17]:

$$\alpha = \frac{\sqrt{2\pi f}}{c} \times \sqrt{(\mu''\varepsilon'' - \mu'\varepsilon') + \sqrt{(\mu''\varepsilon'' - \mu'\varepsilon')^2 - (\mu'\varepsilon'' - \mu''\varepsilon')^2}} \quad (6)$$

$$\sigma = 2\pi f \varepsilon_0 \varepsilon'' \quad (7)$$

$$\delta = \sqrt{\frac{1}{\pi f \mu \sigma}} \quad (8)$$

Where C is the speed of light in vacuum, f denotes the incident wave frequency, σ is the conductivity, and ε_0 represents the electric permeability constant of the vacuum equal to 854.8×10^{-12} F/m. Changes in the damping constant relative to frequency for Ti_3C_2/TiO_2 composites are displayed in Fig. 7(a).

[DOI: 10.22068/ijmse.4035]

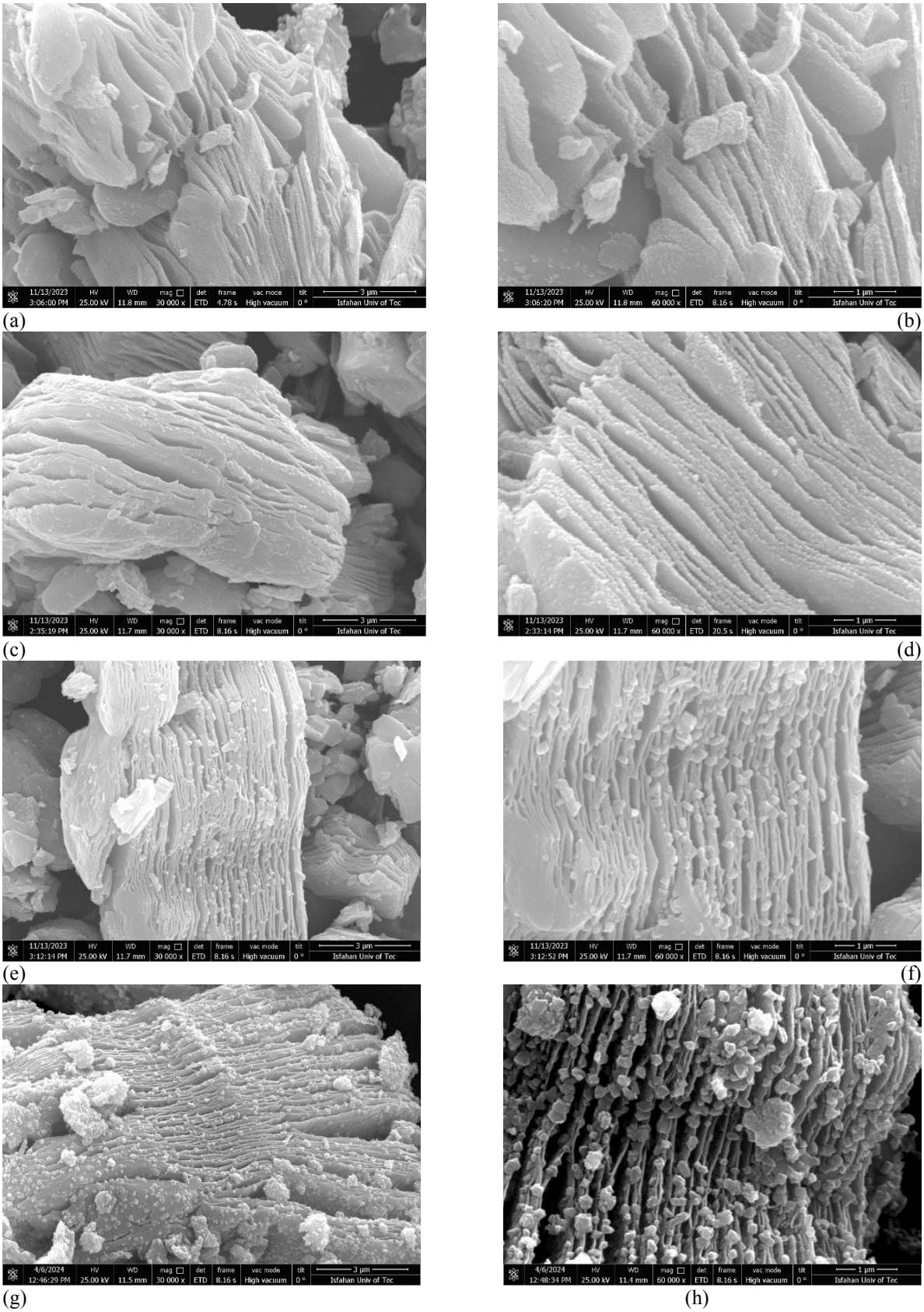

Fig. 5. The SEM micrographs of $Ti_3C_2T_x$ MXene phase after annealing process at, a & b) 500, c & d) 600, e & f) 700 and g & h) 800°C for 2 h

[DOI: 10.22068/ijmse.4035]

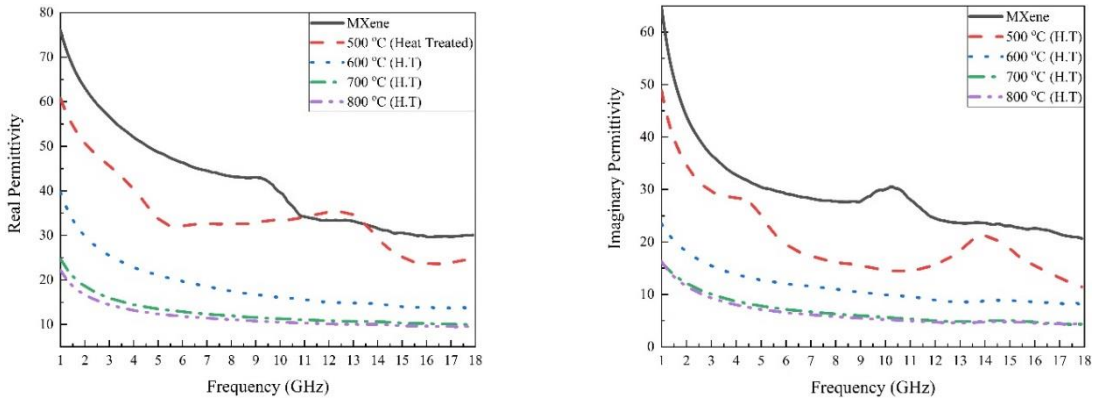

Fig. 6. The changes in a) imaginary and b) real parts of electrical permittivity in relation to frequency (within 1-18 GHz) for $Ti_3C_2T_x$ MXene phase before and after annealing process at different annealing temperatures

Based on equation (6), higher ε" result in a larger α value. Therefore, the highest and lowest values of α parameter correspond to pure $Ti_3C_2T_x$ MXene and annealed samples at 800°C, respectively. It should be noted that the value of parameter α decreases with increasing frequency. In other words, composites prepared at high frequency have higher performance. According to the results presented in Fig. 7(b), the values of δ decrease abruptly in the range of 1–7 GHz, followed by an almost frequency-independent behavior. Based on this figure, it is quite evident that the maximum skin depth is related to Ti_3C_2/TiO_2 composites annealed at 800°C. Reflection loss (RL) is a key parameter that characterizes the absorption characteristics of electromagnetic waves. When RL values are less than -10 dB, 90% of the EM wave energy is absorbed. The EM wave absorption performance of the prepared composites can be confirmed according to transmission line theory with the RL value. It can be calculated by the correlation of complex permeability and complex permeability as follows [9]:

$$RL(dB) = 20\log\left|\frac{Z_{in}-Z_0}{Z_{in}+Z_0}\right| \quad (9)$$

$$Z_{in} = \sqrt{\frac{\mu_r}{\varepsilon_r}}\tanh\left[j\frac{2\pi ft}{c}\sqrt{\mu_r\varepsilon_r}\right] \quad (10)$$

Where Z_{in} is the input characteristic impedance, Z_0 denotes the impedance of free space, d stands for the thickness of the hybrid composite, ε_r shows the complex permittivity, μ_r represents the complex permeability. In this regard, the RL curves of prepared composites at different temperatures within frequency range 1-18 GHz (1-5 mm thicknesses) are illustrated in Fig. 8. As seen, best absorption behavior of EM waves belongs to the annealed sample at 800°C with a thickness of 2 mm with the RL_{min} of about -22 dB at matching frequency of 12 GHz. Meanwhile, the weakest absorption behavior of EM waves, with RL_{min} of about -5.51 dB at matching frequency of 8.95 GHz, is attributed to the pure $Ti_3C_2T_x$ MXene phase.

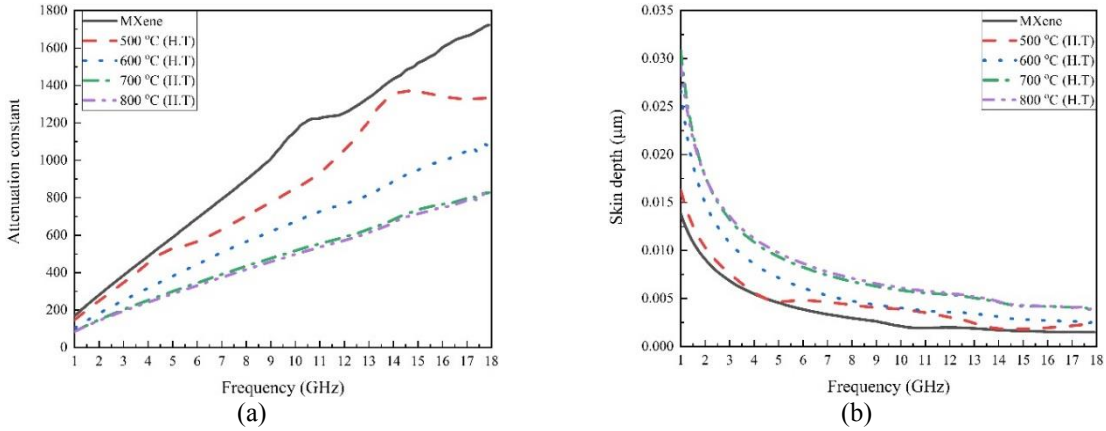

Fig. 7. The changes in a) attenuation constant and b) skin depth in relation to frequency (within 1-18 GHz) for $Ti_3C_2T_x$ MXene phase before and after annealing process at different annealing temperatures

[DOI: 10.22068/ijmse.4035]

Considering that the RL_{min} of composites prepared at temperatures below 500°C (-7.98 dB at the matching frequency of 7.88 GHz) is less than -10 dB, these materials are not suitable for EM absorption. In contrast, performing the annealing process at higher temperatures has been able to increase
the performance of the resulting structures in absorbing electromagnetic waves to an acceptable extent. As seen, the reflection loss (RL) changed from -7.98 to -21.28 dB (within frequency range of 1-18 GHz) with an increase in annealing temperature to about 800°C. This result can be related to the increase in crystalline defects, reduction of interfaces and a suitable percentage of TiO_2 within the Ti_3C_2 sheets. According to Fig. 8, the matching frequencies of prepared composites shift to lower frequencies with increasing sample thickness. The reason is attributed to the spin matching at high frequencies. In fact, the studied samples in this work follow the law of quarter-wavelength weakening as follow [17]:

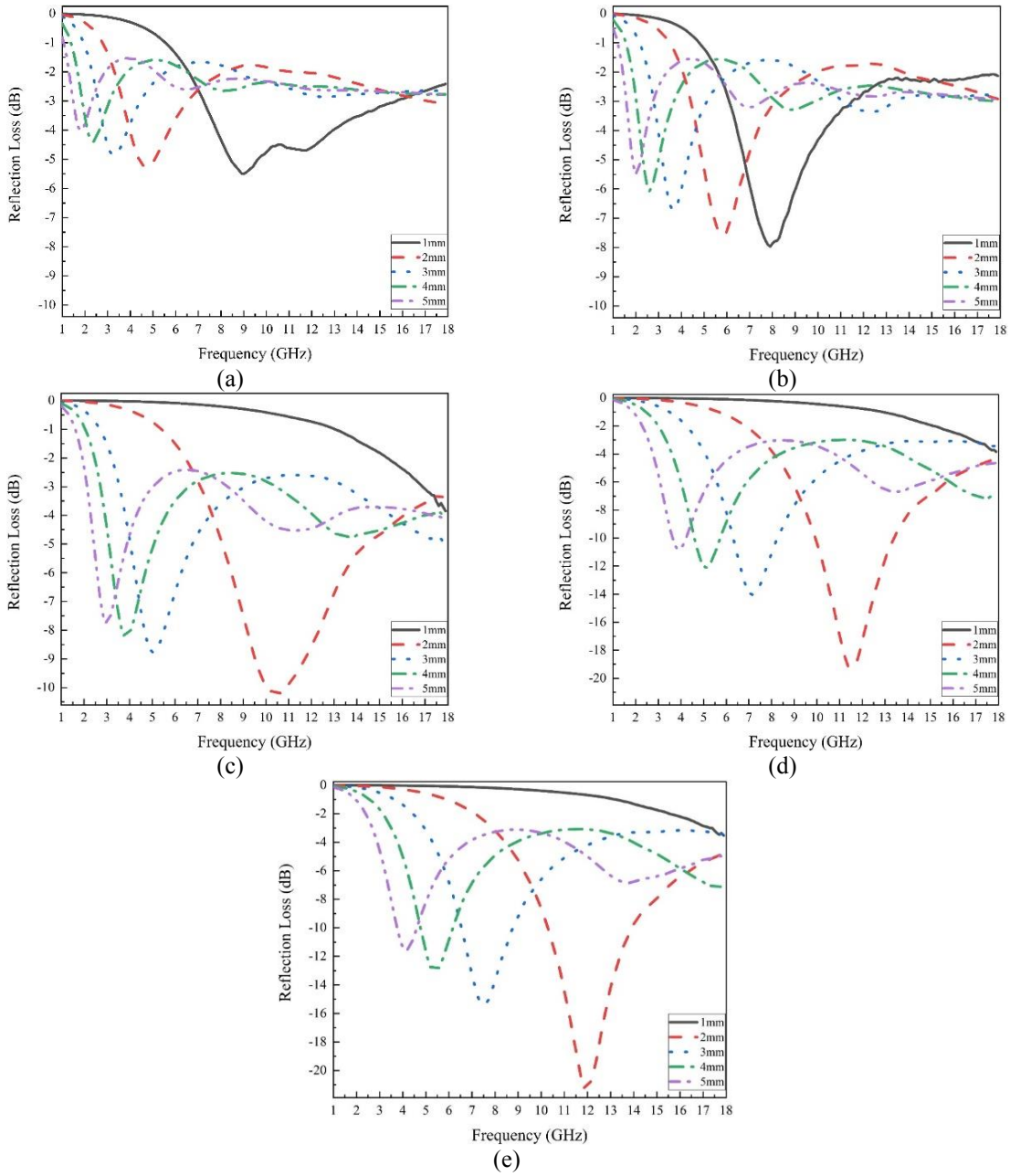

Fig. 8. Reflection loss (RL) curves related to $Ti_3C_2T_x$ MXene phase a) before and after annealing at b) 500, c) 600, d) 700 and e) 800°C for 2 h

[DOI: 10.22068/ijmse.4035]

$$t_m = \frac{n\lambda_m}{4} = \frac{nc}{4f_m\sqrt{|\mu_r||\varepsilon_r|}} \quad (11)$$

In this equation, n= 1, 2, 3, f_m is the frequency corresponding to a particular RL peak, and λ_m denotes the wavelength at f_m [17]. Accordingly, the EM wave absorption function of the mentioned composites can be effectively adjusted by changing the thickness of the sample.

The data presented in Table 1 are used for comparison between the synthesised samples and some advanced ceramics. Evidently, electromagnetic parameters are heavily affected by the chemical composition and microstructure. For example, the Ti_3C_2/TiO_2 composites can be compared with Ti_3SiC_2/Al_2O_3 and $Ti_3C_2T_x$/FCl [25, 26]. However, $Ti_3C_2T_x/Fe_3O_4$, because of the existence of magnetic losses (μ', μ″), shows a better electromagnetic behaviour [27].

Table 1. Comparison of EM wave absorbing properties of materials

Sample	RL_{min} (dB)	Layer thickness (mm)	Ref.
Ti_3SiC_2/Al_2O_3	-16.4	2	[25]
$Ti_3C_2T_x$/FCl	-15.52	1	[26]
$Ti_3C_2T_x/Fe_3O_4$	-57.2	3.6	[27]

4. CONCLUSIONS

The present work is set out with the aim of studying the effect of TiO_2 on the electromagnetic (EM) behaviour of in-situ Ti_3C_2/TiO_2 composites. The results showed that by performing the controlled annealing process, it is possible to deposit the TiO_2 particles within the MXene phase and form the Ti_3C_2/TiO_2 composites in situ. The electromagnetic wave absorbing behaviours of Ti_3C_2/TiO_2 composites are in direct relation with the annealing temperature as a result of the in-situ precipitation of TiO_2 within Ti_3C_2 sheets. The reflection loss (RL) changed from -7.98 to -21.28 dB (within the frequency range of 1-18 GHz) with an increase in annealing temperature, as well as an increase in the size and percentage of formed TiO_2 phase.

ACKNOWLEDGMENTS

I would like to thank Professor Ali Ghasemi for his invaluable feedback and reassurance, which significantly influenced how I conducted my experiments, analysed my results, and interpreted them.

REFERENCES

[1] Wang, Z., Cheng, Z., Fang, C., Hou, X., Xie, L., "Recent advances in MXenes composites for electromagnetic interference shielding and microwave absorption". Composites Part A: Applied Science and Manufacturing, 2020, 136, 105956-105973.

[2] Lim, K.R.G., Shekhirev, M., Wyatt, B.C., Anasori, B., Gogotsi, Y., She, Z.W., "Fundamentals of MXene synthesis". Nature Synthesis, 2022, 1(8), 601-614.

[3] Heidarpour, A., Faraji, M., Haghighi, A., "Production and characterization of carbide-derived-nanocarbon structures obtained by HF electrochemical etching of Ti_3AlC_2". Ceramics International, 2022, 48 (8), 11466-11474.

[4] Shahin, N., Kazemi, Sh., Heidarpour, A., "Mechanochemical synthesis mechanism of Ti_3AlC_2 MAX phase from elemental powders of Ti, Al and C". Advanced Powder Technology, 2016, 27 (4), 1775-1780.

[5] Aghamohammadi, H., Heidarpour, A., Jamshidi, R., Ghasemi, S., "Study on the chemical stability of the synthesized TiC_x in Ti-Al-C system after immersion in the $HF+H_2O_2$ solution". Advanced Powder Technology, 2019, 30 (2), 393-398.

[6] Pan, F., Yu, L., Xiang, Z., Liu, Z., Deng, B., Cui, E., Shi, Z., Li, X., Lu, W., "Improved synergistic effect for achieving ultrathin microwave absorber of 1D Co nanochains/ 2D carbide MXene nanocomposite". Carbon, 2021, 172, 506-515.

[7] Wang, X., Zhao, C., Li, C., Liu, Y., Sun, S., Yu, Q., Yu, B., Cai, M., Zhou, F., "Progress in MXene-based materials for microwave absorption". Journal of Materials Science & Technology, 2024, 180, 207-225.

[8] Guan, X., Yang, Z., Zhou, M., Yang, L., Peymanfar, R., Aslibeiki, B., Ji, G., "2D MXene nanomaterials: Synthesis, mechanism, and multifunctional applications in microwave absorption". Small Structures, 2022, 3(10), 2200102-2200125.

[9] Ghasemi, A., Magnetic Ferrites and Related Nanocomposites, Elsevier, USA, 2022.

[10] Chang, M., Li, Q., Jia, Z., Zhao, W., Wu, G., "Tuning microwave absorption properties of $Ti_3C_2T_x$ MXene-based materials: Component optimization and structure modulation".

[DOI: 10.22068/ijmse.4035]

Journal of Materials Science & Technology, 2023, 148, 150-170.
[11] Kumar, A., Agarwala, V., Singh, D., "Microwave absorbing behavior of metal dispersed TiO_2 nanocomposites". Advanced Powder Technology, 2014, 25 (2), 483-489.
[12] Liu, Z., Zhou, Y., Yang, L., Yang, R., "Green preparation of in-situ oxidized TiO_2/Ti_3C_2 heterostructure for photocatalytic hydrogen production". Advanced Powder Technology, 2021, 32 (12), 4857-4861.
[13] F. Wang, C. Yang, M. Duan, Y. Tang, J. Zhu, TiO_2 nanoparticle modified organ like Ti_3C_2 MXene nanocomposite encapsulating hemoglobin for a mediator-free biosensor with excellent performances, Biosensors and Bioelectronics 74 (2015) 1022-1028.
[14] Tong, Y., He, M., Zhou, Y., Nie, S., Zhong, Q., Fan, L., Huang, T., Liao, Q., Wang, Y., "Three-dimensional hierarchical architecture of the $TiO_2/Ti_3C_2T_x$/RGO ternary composite aerogel for enhanced electromagnetic wave absorption". ACS sustainable chemistry & engineering, 2018, 6 (7), 8212-8222.
[15] Fan, B., Shang, S., Dai, B., Zhao, B., Li, N., Li, M., Zhang, L., Zhang, R., Marken, F., "2D-layered Ti_3C_2/TiO_2 hybrids derived from Ti_3C_2 MXenes for enhanced electromagnetic wave absorption". Ceramics International, 2020, 46 (10), 17085-17092.
[16] Sun, X., Zhao, X., Zhang, X., Wu, G., Rong, X., Wang, X., "TiO_2 nanosheets/ $Ti_3C_2T_x$ MXene 2D/2D composites for excellent microwave absorption", ACS Applied Nano Materials, 2023, 6 (15), 14421-14430.
[17] Yan, H., Guo, Y., Bai, X., Qi, J., Lu, H., "Facile constructing $Ti_3C_2T_x/TiO_2$@C heterostructures for excellent microwave absorption properties". Journal of Colloid and Interface Science, 2024, 654, 1483-1491.
[18] Gao, Y., Du, H., Li, R., Zhang, Q., Fan, B., Zhao, B., Li, N., Wang, X., Chen, Y., Zhang, R., "Multi-phase heterostructures of flower like Ni (NiO) decorated on two-dimensional $Ti_3C_2T_x/TiO_2$ for high-performance microwave absorption properties". Ceramics International, 2021, 47 (8), 10764-10772.
[19] Zamani, K., Tavoosi, M., Ghasemi, A., Gordani, G., "Electromagnetic characterization of MAX phase and MXene in Ti-Al-C ternary system", Materials Chemistry and Physics, 2024, 323, 129622-129632.
[20] Tahir, M., "Nanoconfined Ti_3C_2@ in situ grown TiO_2 and ruthenium triphenyl phosphine (Ru-II) coupled g-C_3N_4 to construct RuP-Ti_3C_2@TiO_2/EC_3N_4 dual function nanocomposite for enhancing photocatalytic green hydrogen production". Chemical Engineering Journal, 2023, 476, 146680-146690.
[21] Tong, Y., He, M., Zhou, Y., Zhong, X., Fan, L., Huang, T., Liao, Q., Wang, Y., "Electromagnetic wave absorption properties in the centimetre-band of $Ti3C2T_x$ MXenes with diverse etching time", Journal of Materials Science: Materials in Electronics, 2018, 29, 8078-8088.
[22] Lei, B., Huang, X., Wu, P., Wang, L., Huang, J., Wang, Z., "Sandwich-like preparation of $Ti_3C_2T_x$/CoFe/TiO_2 nanocomposites for high-performance electromagnetic wave absorption". Ceramics International, 2022, 48 (17), 25111-25119.
[23] Yang, J.X., Yu, W.B., Li, C.F., Dong, W.D., Jiang, L.Q., Zhou, N., Zhuang, Z.P., Liu, J., Hu, J.Y., Zhao, H., "PtO nanodots promoting Ti_3C_2 MXene in-situ converted Ti_3C_2/TiO_2 composites for photocatalytic hydrogen production". Chemical Engineering Journal, 2021, 420, 129695-129704.
[24] Zhou, C., Wang, X., Luo, H., Deng, L., Wei, S., Zheng, Y., Jia, Q., Liu, J., "Rapid and direct growth of bipyramid TiO_2 from $Ti_3C_2T_x$ MXene to prepare Ni/TiO_2/C heterogeneous composites for high-performance microwave absorption". Chemical Engineering Journal, 2020, 383, 123095-123104.
[25] Dai, B., Zhao, B., Xie, X., Su, T., Fan, B., Zhang, R., Yang, R., "Novel two-dimensional $Ti_3C_2T_x$ MXenes/nano-carbon sphere hybrids for high-performance microwave absorption". Journal of Materials Chemistry C, 2018, 6, 5690-5697.
[26] Zhang, X., Wang, H., Hu, R., Huang, C., Zhong, W., Pan, L., Feng, Y., Qiu, T., Zhang, C.J., Yang, J., "Novel solvothermal preparation and enhanced microwave absorption properties of $Ti_3C_2T_x$ MXene modified by in situ coated Fe_3O_4 nanoparticles". Applied Surface Science, 2019, 484, 383-391.
[27] Yan, S., Cao, C., He, J., He, L., Qu, Z.,

[DOI: 10.22068/ijmse.4035]

"Investigation on the electromagnetic and broadband microwave absorption properties of Ti_3C_2 Mxene/flaky carbonyl iron composites". Journal of Materials Science: Materials in Electronics, 2019, 30, 6537-6543.

[28] Zhao, D., Xia, S., Wang, Y., Wang, M., "High-performance microwave absorption properties of Ti_3SiC_2/Al_2O_3 coatings prepared by plasma spraying". Applied Physics A, 2020, 126, 1-9.

[DOI: 10.22068/ijmse.4035]